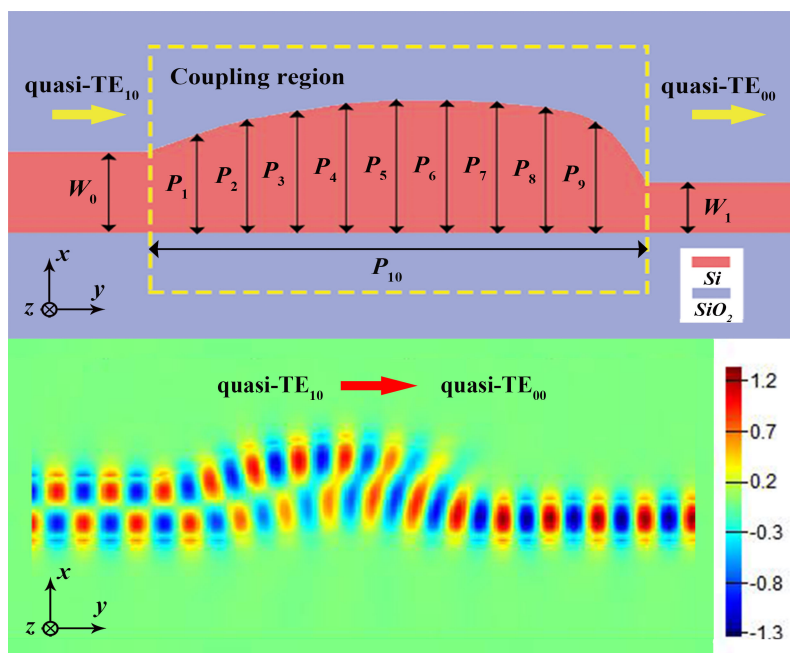


# Ultra-Compact Broadband In-Line Mode Converter Based on a Width-Modulated Silicon Waveguide

Volume 13, Number 2, April 2021

Ze Chen  
Tianying Lin  
Xiaoping Liu  
Haibin Lv



DOI: 10.1109/JPHOT.2021.3066198

# Ultra-Compact Broadband In-Line Mode Converter Based on a Width-Modulated Silicon Waveguide

Ze Chen <sup>1,2</sup> Tianying Lin,<sup>1,2</sup> Xiaoping Liu,<sup>3</sup> and Haibin Lv <sup>3</sup>

<sup>1</sup>National Laboratory of Solid State Microstructures and College of Engineering and Applied Sciences, Nanjing University, Nanjing 210093, China

<sup>2</sup>Collaborative Innovation Center of Advanced Microstructures, Nanjing University, Nanjing, Jiangsu 210093, China

<sup>3</sup>School of Physical Science and Technology, ShanghaiTech University, Shanghai 201210, China

DOI:10.1109/JPHOT.2021.3066198

This work is licensed under a Creative Commons Attribution 4.0 License. For more information, see <https://creativecommons.org/licenses/by/4.0/>

Manuscript received January 13, 2021; revised March 10, 2021; accepted March 11, 2021. Date of publication March 17, 2021; date of current version April 8, 2021. This work was supported in part by the Shanghai Municipal Science and Technology Major Project under Grant 2017SHZDZX03 and in part by the National Basic Research Program of China under Grant 2015CB659400. Corresponding authors: Xiaoping Liu; Haibin Lv (e-mail: liuxp1@shanghaitech.edu.cn; lvhaibin203@163.com).

**Abstract:** Mode division multiplexing (MDM) technology is becoming increasingly important for modern optical communication systems. Here, an ultra-compact broadband in-line mode converter for quasi-TE<sub>00</sub> and quasi-TE<sub>10</sub> on the silicon-on-insulator platform is proposed and demonstrated experimentally. In our device, the mode-conversion region consists of a continuously width-modulated waveguide with a footprint size as small as  $1.32 \times 4.52 \mu\text{m}^2$ . Its modulation profile is designed by using the particle swarm optimization algorithm. This device has a simulated conversion efficiency of about  $-0.174$  dB and an insertion loss less than  $0.153$  dB within 100-nm wavelength bandwidth from 1500 nm to 1600 nm. Our design exhibits a favorable fabrication error tolerance and the fabricated device has achieved nearly the same conversion efficiency as the simulated one. Our concept can also be applied to design other high-performance mode converters, i.e., converting modes between quasi-TE<sub>20</sub> and quasi-TE<sub>00</sub>. Our work suggests a very promising path for realizing compact integrated MDM systems.

**Index Terms:** Mode converter, particle swarm optimization, silicon waveguide.

## 1. Introduction

Multiplexing technology, transmitting several signals in shared channels, can greatly enhance the information transmission capacity, e.g., in optical fiber systems, photonic integrated circuits (PICs), and wireless communication systems. Wavelength division multiplexing (WDM) [1], [2] with low crosstalk has already gained great success in offering broad operation bandwidth and increasing the channel capacity. In recent years, while the transmission capacity based on dense wavelength division multiplexing (DWDM) technology has become increasingly saturated, mode division multiplexing (MDM) [3] in fiber systems and chip-based systems provides another effective approach. In a waveguide system, MDM leverages the orthogonality of different eigen-modes of the waveguide, each of which can carry data independently in an ideal case. One of the key components in an MDM system is mode converters for converting one mode to another. In PICs, the mode converter

consists of polarization rotators (PRs) [4], [5] and mode-order converters. The polarization handling devices, such as PRs, are used to minimize the polarization-dependent dispersion and loss [6], while the mode-order converters are more important especially when the input of some systems [7] should be high-order modes. Various interesting schemes of the mode-order converter have been reported. In the early years, on-chip tilted Bragg gratings were introduced to implement the mode-order conversion, but their large dimension of  $14 \times 5000 \mu\text{m}^2$  and narrow bandwidth of roughly 0.5 nm hinder the large-scale integration of SOI MDM photonic systems [8]. Different mode converters were also demonstrated with a reduced footprint, for example, Mach-Zehnder interferometer (MZI) [9] with a footprint of  $5 \times 15 \mu\text{m}^2$ , an insertion loss of 0.4 dB and a bandwidth of 100 nm, and directional coupler [10] with a footprint of  $6 \times 25 \mu\text{m}^2$ , an insertion loss of 1 dB, and a bandwidth of 20 nm. Mode conversion was also realized using dielectric meta-structures with subwavelength periodic perturbations [11], and the total device size was  $1.1 \times 6.736 \mu\text{m}^2$  with an insertion loss of less than 1.5 dB.

Here, we demonstrate an ultra-compact and highly efficient waveguide-width-modulated in-line mode converter on the SOI photonic platform. This converter, converting modes between quasi- $\text{TE}_{00}$  and quasi- $\text{TE}_{10}$ , is inversely designed and optimized by particle swarm optimization (PSO) [12]–[14]. Its footprint is  $1.32 \times 4.52 \mu\text{m}^2$  and insertion loss is less than 0.153 dB. Our results suggest that the physical mechanism behind the mode conversion between quasi- $\text{TE}_{00}$  mode and quasi- $\text{TE}_{10}$  mode can be attributed to the establishment of the  $\pi$  phase difference between the two lobes of the electric field of quasi- $\text{TE}_{10}$  mode. It is achieved by using the asymmetric width modulation that leads to a differential path length for the two lobes. The physical mechanism can also be applied to design other mode converters converting quasi- $\text{TE}_{00}$  mode to other high order modes. Our concept here provides an effective and feasible approach to pursue a device-design scheme that allows for a much compact footprint and potentially broad operation bandwidth, shedding light on the possibility of realizing a high-performance MDM system.

## 2. Design and Performance of Quasi- $\text{TE}_{00}$ to Quasi- $\text{TE}_{10}$ Mode Converter

Traditional mode couplers require phase matching condition or quasi phase matching condition that can be fulfilled by engineering waveguide dispersion or using an optical grating. The common theoretical framework, i.e., coupled mode theory, for designing and analyzing these devices, is based on a slowly varying envelope approximation, under which the second-order differential Maxwell equations are transformed to the first-order differential coupled mode equations. Devices designed based on this theoretical framework falls into a weak coupling situation [15], which in turn leads to a long mode interaction distance, in other words, a large device footprint. Our proposed mode-converting structure, however, does not necessarily fall into the weak coupling cases. This is because our design method, enabled by particle swarm optimization (PSO) algorithm and coupled with 3D finite-difference time-domain (FDTD), naturally allows for searching a much large parameter space, including the strong coupling region. An exemplified in-line mode converter is shown in Fig 1(a), which is designed on a silicon-on-insulator platform with a 220 nm top silicon layer covered by  $\text{SiO}_2$  upper-cladding. It converts quasi- $\text{TE}_{00}$  mode (an even mode) to quasi- $\text{TE}_{10}$  mode (an odd mode) and vice versa. Along the direction of light propagation, the device design is composed of three parts: the input waveguide, the coupling waveguide, and the output waveguide. Here, the width of the input waveguide and output waveguide is  $W_0 = 800$  nm and  $W_1 = 500$  nm, respectively, and the coupling waveguide has a straight side and a curved side to break the symmetry along the propagation direction, i.e., y-axis in our case. This symmetry breaking is crucial for converting modes with different parities here. In our design, the coupling waveguide is first divided into 9 pieces with their width labeled as  $P_i$  ( $i = 1, \dots, 9$ ) in Fig. 1(a) and its length is set to  $P_{10}$ . Spline interpolation is then used to obtain a continuous curve for the curved side, and for example, in the zoom-in view of one discrete section, there are 9 spline interpolating points, represented by  $s(p)$  ( $p = 1, \dots, 9$ ), to connect adjacent discrete optimized points. The last 3D finite-difference time-domain (FDTD) method driven by particle swarm optimization (PSO) algorithm is used to optimize the device for maximum averaged conversion efficiency from quasi- $\text{TE}_{10}$  to quasi- $\text{TE}_{00}$

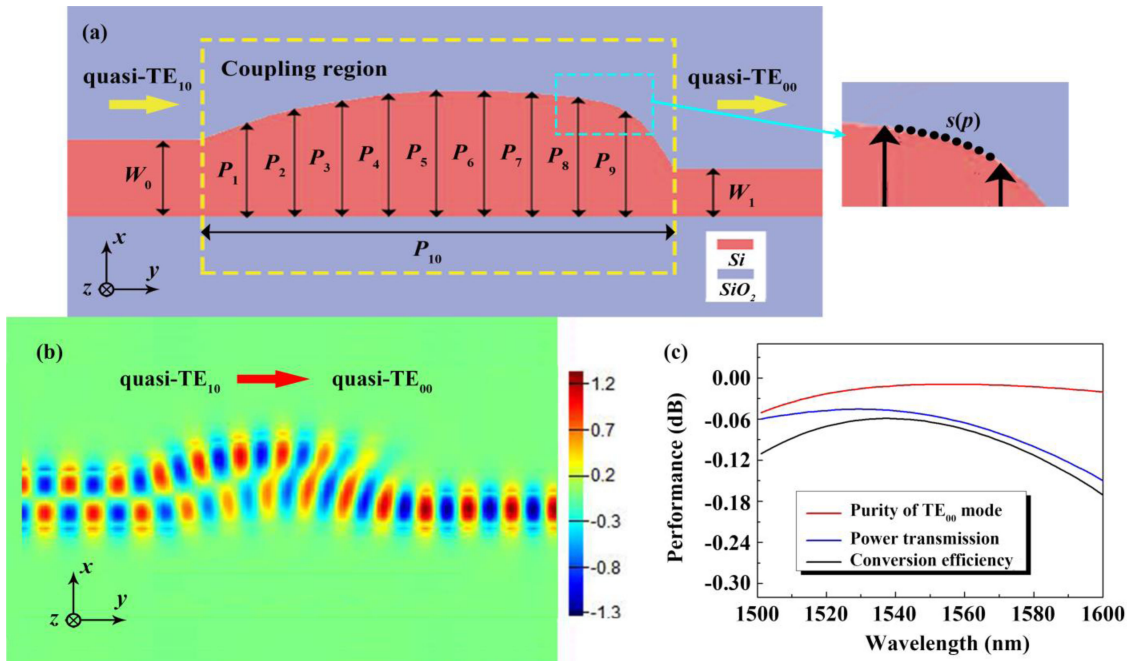


Fig. 1. (a) Schematic of our proposed mode converter between quasi-TE<sub>10</sub> and quasi-TE<sub>00</sub> modes. In the coupling region,  $P_i$  ( $i = 1, \dots, 9$ ) denotes the width of different sections which determines the curve shape of the coupling region by spline interpolation, and  $P_{10}$  is the length of the coupling region.  $W_0$  and  $W_1$  are the width of the input waveguide and output waveguide, respectively. In the zoom-in view,  $s(p)$  ( $p = 1, \dots, 9$ ) denotes the positions of the spline interpolating points in one discrete section, which transforms the discrete boundary into a quasi-continuous one. (b) The simulated major transverse electric field distribution at a wavelength of 1550 nm. (c) The simulated performance of the mode converter within a wavelength range from 1500 nm to 1600 nm.

TABLE 1  
Geometric Parameters of Our Proposed Mode Converter Between Quasi-TE<sub>10</sub> and Quasi-TE<sub>00</sub> Modes

Parameter	$W_0$	$W_1$	$P_1$	$P_2$	$P_3$	$P_4$	$P_5$
Value ( $\mu\text{m}$ )	0.800	0.500	0.976	1.120	1.202	1.275	1.315
Parameter	$P_6$	$P_7$	$P_8$	$P_9$	$P_{10}$		
Value ( $\mu\text{m}$ )	1.310	1.284	1.234	1.096	4.525		

within a given wavelength range. We set the mesh accuracy of the 3D FDTD simulation to 18 points per wavelength (PPW), and use the perfectly matched layer (PML) as its boundary conditions. Especially, the maximum mesh step in the mesh override region of the coupling waveguide is set to  $0.01 \mu\text{m}$ . The resulted mode converter structure parameters are summarized in Table 1. This device is extremely compact with its footprint size of about  $1.32 \times 4.52 \mu\text{m}^2$ . To illustrate the mechanism behind our design, the corresponding major transverse electric field distribution for the wavelength of 1550 nm is depicted in Fig. 1(b). When the quasi-TE<sub>10</sub> mode enters the coupling region in the middle, the two field lobes of the quasi-TE<sub>10</sub> mode, having an initial  $\pi$  phase difference, will take different paths, one approximately following the upper edge of the coupling region while the other following the lower edge. Since the upper edge is curved, in other words, has a longer path, the lobe taking the upper edge experiences a longer propagation phase delay than the other lobe. When the  $\pi$  phase delay is induced, the initial phase difference of the two lobes will be eliminated and the field emerges as a single lobe and couples into the quasi-TE<sub>00</sub> mode.

TABLE 2  
Detailed Parameters for the Mode (de)Multiplexer

Width of bus waveguide (nm)	Width of access waveguide (nm)	Gap (nm)	Coupling length ( $\mu\text{m}$ )
$W_b$	$W_a$	$L_g$	$L_c$
800	500	100	7

The simulated performance of our designed in-line mode converter is summarized in Fig. 1(c). The maximum power transmission of this device is  $-0.046$  dB (98.95%) at 1527 nm, while the transmission keeps above  $-0.153$  dB (96.54%) within the 1500-1600 nm wavelength range as indicated by the blue solid line. Furthermore, the black solid line represents the mode conversion efficiency between quasi-TE<sub>00</sub> and quasi-TE<sub>10</sub>, which keeps above  $-0.174$  dB (96.07%) within the same wavelength range and reaches the highest value of  $-0.059$  dB (98.65%) at 1537 nm. Moreover, the purity of quasi-TE<sub>00</sub> mode, indicated by the red solid line, as another important performance factor for the mode converter, is as high as  $-0.01$  dB (99.77%) at the 1553 nm wavelength, and the degradation of purity is less than 0.041 dB over the 100-nm wavelength bandwidth. Compared with the results in previous literature [16]–[20], our proposed mode converter has not only a much compact footprint but also advantages in terms of insertion loss and conversion efficiency.

### 3. Experiment and Result

The in-line mode converter between quasi-TE<sub>10</sub> and quasi-TE<sub>00</sub> modes is fabricated on a silicon-on-insulator (SOI) wafer with a 220 nm top silicon layer on a 2  $\mu\text{m}$  buried silicon-dioxide layer by a single step of electron beam lithography and inductively coupled plasma (ICP) etching. The scanning electron micrograph (SEM) image of a typical device before SiO<sub>2</sub> cladding deposition is shown in Fig. 2(a). The geometric shape of the fabricated mode converter agrees well with our design. In general, evaluating the in-line mode converter efficiency by directly comparing the modal power before and after conversion encounters serious difficulties due to the lack of direct on-chip modal power measurement methods. Fig. 2(b) shows the experiment flow of our alternative indirect measurement method. Here, the insertion loss of three devices is characterized via grating coupling with a tunable external cavity laser (Santec TSL-710), a polarization controller (to maximum the transmitted power) and a photodetector. The first one is a grating coupled short reference waveguide section and its insertion loss is denoted as  $L_1$ . The second one is a grating coupled quasi-TE<sub>10</sub> mode multiplexer followed by a demultiplexer (both made of the same directional couplers (DC) [21], [22]) and the overall insertion loss is denoted as  $L_2$ . Detailed parameters for this mode (de)multiplexer are shown in Table 2. According to Lorentz reciprocity theorem [23], these two symmetrically placed (de)multiplexers would show exactly the same (de)multiplexing insertion loss, which can be expressed as  $L_{mux} = (L_2 - L_1)/2$ . Its corresponding measured result is shown in Fig. 2(c). Within the 1500-1600 nm wavelength range, it is less than 3.69 dB. The final one contains our designed mode converter and a quasi-TE<sub>10</sub> mode demultiplexer. The overall insertion loss of this device is denoted as  $L_3$ , which can also be expressed as

$$L_3 = L_1 + L_{mux} + L_{conv} \quad (1)$$

Here,  $L_{conv}$  represents the insertion loss or mode conversion efficiency of our in-line mode converter designed to convert modes between quasi-TE<sub>00</sub> and quasi-TE<sub>10</sub>. Its experimentally measured data are plotted in Fig. 2(d) as the red solid line. Within the 100-nm wavelength bandwidth, the conversion efficiency of our device exceeds  $-0.830$  dB and reaches a maximum value of  $-0.095$  dB near 1555 nm. The oscillatory behavior of the curve is mainly due to the subtle insertion loss oscillation of the quasi-TE<sub>10</sub> mode (de)multiplexer as shown in Fig. 2(c). Furthermore, the blue dash-dotted line represents the fitted value of the experimental results, which is obtained



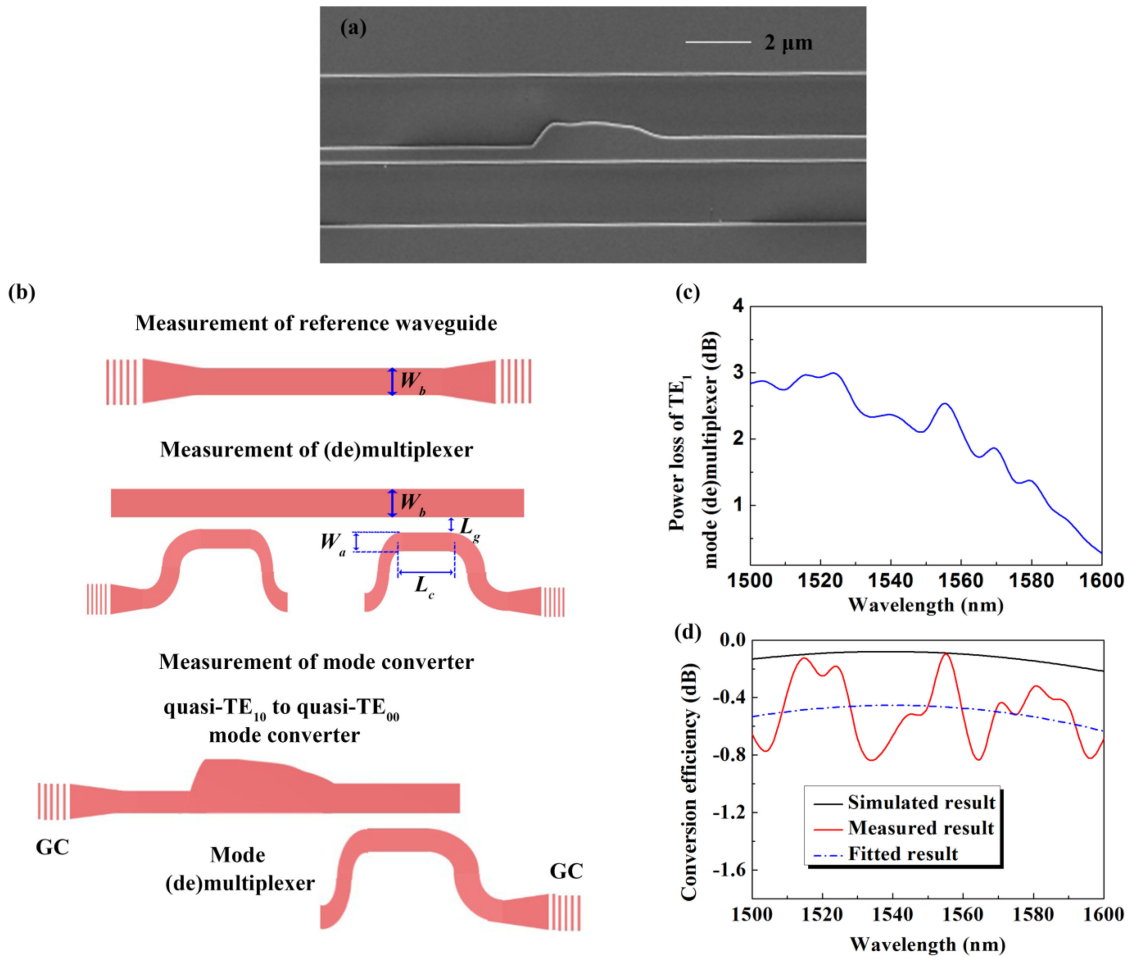


Fig. 2. (a) The SEM image of a typically fabricated in-line mode converter between quasi- $TE_{10}$  and quasi- $TE_{00}$  modes before  $SiO_2$  cladding deposition. (b) The schematic of our alternative indirect measurement method. First, a reference waveguide; Second, a pair of (de) multiplexers for quasi- $TE_{10}$  mode; Third, an in-line mode converter and a quasi- $TE_{10}$  mode demultiplexer. (c) The measured power loss of the  $TE_{10}$  mode (de) multiplexer within 1500-1600 nm wavelength range. (d) The measured conversion efficiency of the fabricated mode converter and its fitted result in comparison with the simulated result.

by the second-order polynomials. It can be compared with the simulated conversion efficiency reproduced from Fig. 1(c) and plotted as the black solid line. The overall trend of the two lines is all mostly identical. Their small discrepancy about 0.4 dB may be attributed to the fabrication errors of this compact mode converter.

#### 4. Discussion

The physical mechanism behind the aforementioned mode converter is widely applicable and thus can be well applied to investigate other cases. For instance, using the exact same design principle, an in-line mode converter converting modes between quasi- $TE_{00}$  and quasi- $TE_{20}$  can be realized on the same SOI wafer as shown in Fig. 3(a). The electric field of quasi- $TE_{20}$  mode has three lobes and the phase between the middle lobe and the rest of the two lobes is different by  $\pi$ . Therefore, our coupling structure for our quasi- $TE_{20}$  and quasi- $TE_{00}$  mode converter is symmetry about the propagation direction, i.e., y-axis in our case. The geometric parameters for our optimized device are listed in Table 3. Its overall footprint is about  $2.5 \times 6.5 \mu m^2$ . Fig. 3(b) reveals the corresponding

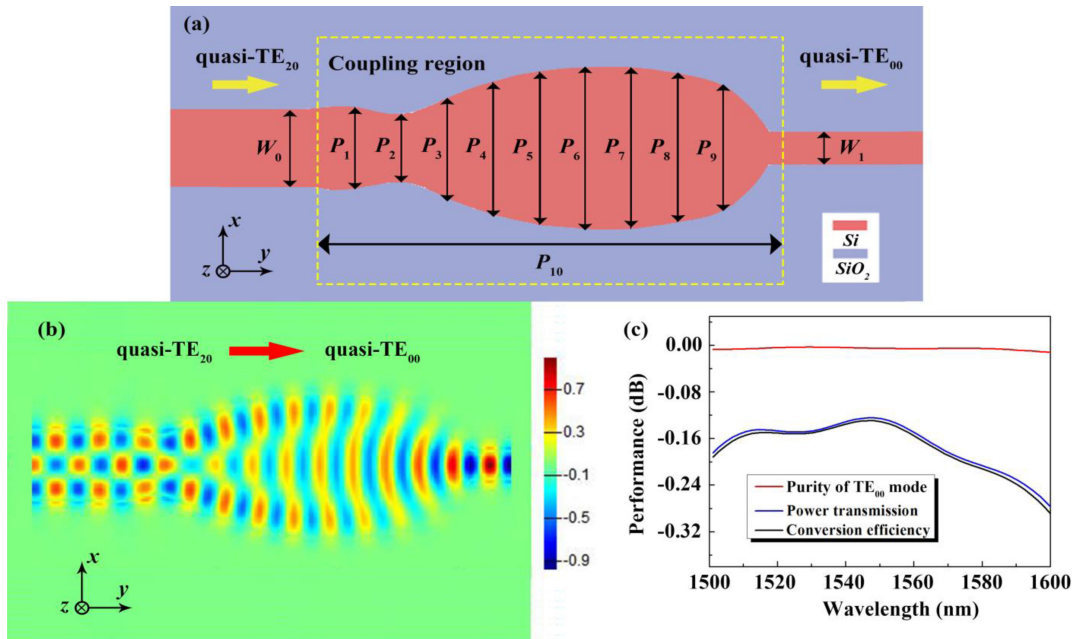


Fig. 3. (a) Schematics of our proposed in-line quasi-TE<sub>20</sub> and quasi-TE<sub>00</sub> mode converter.  $P_i$  ( $i = 1, 2, \dots, 9$ ) represents the width of different sections of the coupling region that determine the shape of the coupling region by spline interpolation, and  $P_{10}$  is the length of the coupling region.  $W_0$  and  $W_1$  represent the width of the input waveguide and output waveguide, respectively. (b) The simulated major transverse field distribution at the wavelength of 1550 nm. (c) The simulated performance of our quasi-TE<sub>20</sub> and quasi-TE<sub>00</sub> mode converter within the wavelength range from 1500 to 1600 nm.

TABLE 3

Geometric Parameters of the In-Line Quasi-TE<sub>20</sub> and Quasi-TE<sub>00</sub> Mode Converter

Parameter	$W_0$	$W_1$	$P_1$	$P_2$	$P_3$	$P_4$	$P_5$
Value ( $\mu\text{m}$ )	1.200	0.500	1.268	1.039	1.556	2.054	2.374
Parameter	$P_6$	$P_7$	$P_8$	$P_9$	$P_{10}$		
Value ( $\mu\text{m}$ )	2.486	2.500	2.300	1.946	6.546		

major transverse electric field distribution for the conversion between TE<sub>00</sub> mode and TE<sub>02</sub> mode at the wavelength of 1550 nm. This again confirms our proposed mode-converting mechanism, where the phase difference between lobes is eliminated by differential path lengths. Its performance is summarized in Fig. 3(c). The power transmission, the conversion efficiency, and the purity of quasi-TE<sub>00</sub> mode are plotted as the blue solid line, the black solid line, and the red solid line, respectively. When a quasi-TE<sub>20</sub> mode is launched into the input waveguide, the power transmission reaches  $-0.124$  (97.18%) at 1547 nm and keeps above  $-0.283$  dB (93.69%) within the 1500-1600 nm wavelength range. The conversion efficiency keeps above  $-0.295$  dB (93.43%) and reaches a maximum value of  $-0.129$  dB (97.07%) at 1546 nm. It can be seen that the power transmission curve and the conversion efficiency curve almost coincide, indicating a very high mode purity of our mode converter. Our further analysis shows that the mode purity is more than  $-0.007$  dB (99.84%) in the 1500-1600 nm wavelength range, and its degradation over the entire wavelength bandwidth is less than 0.004 dB, confirming that the transmitted light is almost a pure mode.

## 5. Conclusion

We have proposed and experimentally demonstrated an in-line broadband mode converter by using continuously width-modulated coupling region. This unique mode coupling region design is enabled

by advanced optimization algorithm and is beyond the traditional framework of coupled mode theory and thus gives rise to a very compact device footprint. The physical mechanism behind this kind of device has its root in differential phase elimination (or generation depending the mode converting direction) by device structure induced differential light paths. In one example, we are able to demonstrate ultra-compact quasi-TE<sub>10</sub> and quasi-TE<sub>00</sub> mode converter with a footprint size of  $1.32 \times 4.52 \mu\text{m}^2$  with very satisfactory experimental performance in the wavelength range from 1500nm to 1600 nm, including its conversion efficiency better than  $-0.830$  dB. Our discovered physical mechanism that enables the compact designing of mode converter are widely applicable. We believe integrated mode-division-multiplexing systems can benefit from our demonstrated devices and most importantly from our design principle.

## References

- [1] B. G. Lee *et al.*, "Ultrahigh-bandwidth silicon photonic nanowire waveguides for on-chip networks," *IEEE Photon. Technol. Lett.*, vol. 20, no. 6, pp. 398–400, Mar. 2008.
- [2] L. W. Luo *et al.*, "WDM-compatible mode-division multiplexing on a silicon chip," *Nature Commun.*, vol. 5, pp. 1–7, 2014, doi: [10.1038/ncomms4069](https://doi.org/10.1038/ncomms4069).
- [3] Y. Ding, J. Xu, F. Da Ros, B. Huang, H. Ou, and C. Peucheret, "On-chip two-mode division multiplexing using tapered directional coupler-based mode multiplexer and demultiplexer," *Opt. Exp.*, vol. 21, no. 8, 2013, Art. no. 10376.
- [4] M. V. Kotlyar, L. Bolla, M. Midrio, L. O'Faolain, and T. F. Krauss, "Compact polarization converter in inorganic material," *Opt. Exp.*, vol. 13, no. 13, 2005, Art. no. 5040.
- [5] M. R. Watts and H. A. Haus, "Integrated mode-evolution-based polarization rotators," *Opt. Lett.*, vol. 30, no. 2, 2005, doi: [10.1364/ol.30.000138](https://doi.org/10.1364/ol.30.000138).
- [6] M. G. Saber *et al.*, "Integrated polarisation handling devices," *IET Optoelectron.*, vol. 14, no. 3, pp. 109–119, 2020.
- [7] A. Liu *et al.*, "Enhanced modal coupling loss in a two-mode SOI waveguide of broken parity-time symmetry," *IEEE Photon. J.*, vol. 10, no. 6, Dec. 2018.
- [8] J. M. Castro, D. F. Geraghty, S. Honkanen, C. M. Greiner, D. Lazikov, and T. W. Mossberg, "Demonstration of mode conversion using anti-symmetric waveguide Bragg gratings," *Opt. Exp.*, vol. 13, no. 11, 2005, Art. no. 4180.
- [9] D. Dai, J. Wang, and Y. Shi, "Silicon mode (de)multiplexer enabling high capacity photonic networks-on-chip with a single-wavelength-carrier light," *Opt. Lett.*, vol. 38, no. 9, 2013, Art. no. 1422.
- [10] Y. Huang, G. Xu, and S. T. Ho, "An ultracompact optical mode order converter," *IEEE Photon. Technol. Lett.*, vol. 18, no. 21, pp. 2281–2283, Nov. 2006, doi: [10.1109/LPT.2006.884886](https://doi.org/10.1109/LPT.2006.884886).
- [11] H. Wang, Y. Zhang, Y. He, Q. Zhu, L. Sun, and Y. Su, "Compact silicon waveguide mode converter employing dielectric metasurface structure," *Adv. Opt. Mater.*, vol. 7, no. 4, pp. 1–6, 2019, doi: [10.1002/adom.201801191](https://doi.org/10.1002/adom.201801191).
- [12] C. Sun, Y. Yu, G. Chen, and X. Zhang, "Ultra-compact bent multimode silicon waveguide with ultralow inter-mode crosstalk," *Opt. Lett.*, vol. 42, no. 15, 2017, Art. no. 3004.
- [13] Z. D. Cheng, Y. L. He, B. C. Du, K. Wang, and Q. Liang, "Geometric optimization on optical performance of parabolic trough solar collector systems using particle swarm optimization algorithm," *Appl. Energy*, vol. 148, pp. 282–293, 2015, doi: [10.1016/j.apenergy.2015.03.079](https://doi.org/10.1016/j.apenergy.2015.03.079).
- [14] Z. H. Ruan, Y. Yuan, X. X. Zhang, Y. Shuai, and H. P. Tan, "Determination of optical properties and thickness of optical thin film using stochastic particle swarm optimization," *Sol. Energy*, vol. 127, pp. 147–158, 2016, doi: [10.1016/j.solener.2016.01.027](https://doi.org/10.1016/j.solener.2016.01.027).
- [15] E. D. By Paul F. Li Ao, and P. L. K. Lincoln, *Theory of Dielectric Optical Waveguides*, 2nd ed., New York, NY, USA: Academic, 1991.
- [16] V. Liu, D. A. B. Miller, and S. Fan, "Ultra-compact photonic crystal waveguide spatial mode converter and its connection to the optical diode effect," *Opt. Exp.*, vol. 20, no. 27, 2012, Art. no. 28388, doi: [10.1364/oe.20.028388](https://doi.org/10.1364/oe.20.028388).
- [17] B.-T. Lee and S.-Y. Shin, "Mode-order converter in a multimode waveguide," *Opt. Lett.*, vol. 28, no. 18, 2003, Art. no. 1660.
- [18] B. E. Abu-elmaaty, M. S. Sayed, R. K. Pokharel, and H. M. H. Shalaby, "General silicon-on-insulator higher-order mode converter based on substrip dielectric waveguides," *Appl. Opt.*, vol. 58, no. 7, 2019, Art. no. 1763.
- [19] L. H. Frandsen *et al.*, "Topology optimized mode conversion in a photonic crystal waveguide fabricated in silicon-on-insulator material," *Opt. Exp.*, vol. 22, no. 7, 2014, Art. no. 8525.
- [20] D. Zhu, H. Ye, Z. Yu, J. Li, F. Yu, and Y. Liu, "Design of compact TE-polarized mode-order converter in silicon waveguide with high refractive index material," *IEEE Photon. J.*, vol. 10, no. 6, 2018, Art. no. 6602907, doi: [10.1109/JPHOT.2018.2883209](https://doi.org/10.1109/JPHOT.2018.2883209).
- [21] Y. Ding, C. Peucheret, and H. Ou, "Ultra-high-efficiency apodized grating coupler using a fully etched photonic crystal," *Pacific Rim Conf. Lasers Electro-Opt., - Tech. Dig.*, vol. 38, no. 15, pp. 2732–2734, 2013, doi: [10.1109/CLEOPR.2013.6599991](https://doi.org/10.1109/CLEOPR.2013.6599991).
- [22] D. Dai, "Advanced passive silicon photonic devices with asymmetric waveguide structures," *Proc. IEEE*, vol. 106, no. 12, pp. 2117–2143, 2018, doi: [10.1109/JPROC.2018.2822787](https://doi.org/10.1109/JPROC.2018.2822787).
- [23] D. Jalas *et al.*, "What is-and what is not-an optical isolator," *Nature Photon.*, vol. 7, no. 8, pp. 579–582, 2013, doi: [10.1038/nphoton.2013.185](https://doi.org/10.1038/nphoton.2013.185).